IEEE Photonics Journal
An IEEE Photonics Society Publication

Open Access

Millimeter-Wave Signal Generation With Tunable Frequency Multiplication Factor by Employing UFBG-Based Acousto-Optic Tunable Filter

Volume 9, Number 1, February 2017

Yiqun Wang
Li Pei
Jing Li
Yueqin Li

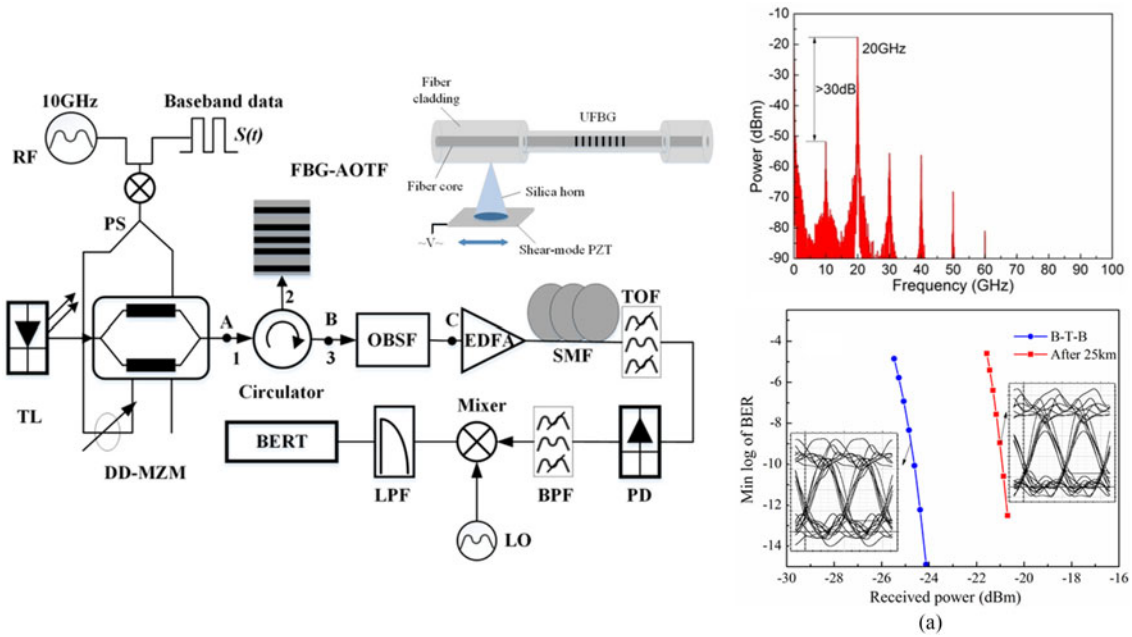

DOI: 10.1109/JPHOT.2017.2651982
1943-0655

Millimeter-Wave Signal Generation With Tunable Frequency Multiplication Factor by Employing UFBG-Based Acousto-Optic Tunable Filter

Yiqun Wang, Li Pei, Jing Li, and Yueqin Li

Key Laboratory of All Optical Network and Advanced Telecommunication Network, Institute of Lightwave Technology, Beijing Jiaotong University, Beijing 100044, China

DOI:10.1109/JPHOT.2017.2651982

Manuscript received October 20, 2016; revised January 5, 2017; accepted January 9, 2017. Date of publication January 16, 2017; date of current version February 6, 2017. This work was supported by the National Natural Science Foundation of China under Grant 61525501. Corresponding author: L. Pei (e-mail: lipei@bjtu.edu.cn).

Abstract: In this paper, a simple and cost-effective millimeter-wave (mm-wave) signal generator with tunable frequency multiplication factor (FMF) by employing the uniform fiber Bragg grating based acousto-optic tunable filter (UFBG-AOTF) is proposed and demonstrated. A dual-driving Mach–Zehnder modulator (MZM) is used to generate multisidebands. The UFBG-AOTF can select the target sidebands. A tunable FMF of even times can be achieved by adjusting the frequency of the applied acoustic wave on the UFBG. Two homemade UFBG-AOTFs are used in a basic radio-over-fiber (RoF) system, resulting in the generation of mm-waves with the FMF of 2 and 4, separately. Moreover, higher FMFs of 6, 8, and 10 are also obtained by simulation. It turns out that after the data transmitting through the SMF of 25 km, the corresponding power penalties are less than 3.8 dB by employing the two homemade FBG-AOTFs. Numerical analysis, simulations, and some experiments are carried out to investigate the mechanism.

Index Terms: Radio over fiber (RoF), millimeter-wave (mm-wave), frequency multiplication factor (FMF), uniform fiber Bragg grating (UFBG), acousto-optic tunable filter (AOTF).

1. Introduction

In the future access services of wireless telecommunication, the radio-over-fiber (RoF) system is very attractive to meet the increasing demands of wide bandwidth, large capacity, low power consumption, high immunity to electromagnetic interferences, as well as system cost-effectiveness [1], [2]. RoF, the integration of wireless and optical systems, takes full advantage of the greater bandwidth provided by the millimeter-wave (mm-wave) frequency resource [3]–[6].

A key technology for an RoF system is the generation of microwave and mm-wave signals. Many optical generation approaches have been reported recently [7]. Among all schemes, optical external modulation can easily and accurately generate high frequency optical microwave and shows great potential for producing 40∼60 GHz optical mm-wave signals [8], [9]. To achieve a high frequency multiplication factor, external modulation techniques employing cascaded or structurized Mach-Zehnder modulator (MZM) were proposed to produce two optical sidebands. The sidebands have a frequency spacing corresponding to multiplication factor times the frequency of the microwave

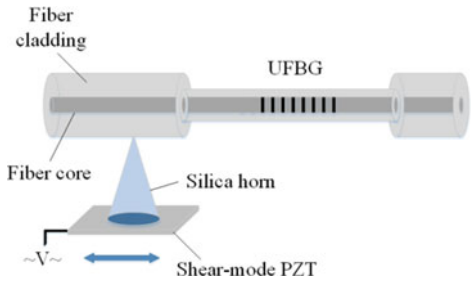

Fig. 1. Conceptual and experimental setup of the UFBG-AOTF.

driving signals. In [10], multiple frequency (2^n of RF frequency) mm-wave signals were produced by using multi-cascaded n external intensity modulators, but this method needs precise control of the phase relation between RF signals on the external modulators. In [11]–[13], quadrupling or octupling mm-wave signals were generated by using an integrated nested MZM. In addition, two schemes were proposed using three parallel MZMs [14] and two parallel dual-parallel MZMs [15], which can be employed 18-tupling and 16-tupling mm-wave signal generation, respectively. The external modulation approaches employing structurized MZMs have a good performance of the optical sideband suppression ratio (OSSR) and a high spectral purity of the generated mm-wave signals, but suffer from poor stability and high complexity. It should be mentioned that the FMF can't be tuned conveniently in the schemes refered above.

Recently, all fiber acousto-optic tunable filter (AOTF) has attracted much attention due to the advantages of wide tuning range, relatively low insertion loss and simple fabrication process [16]. Since a fiber Bragg grating based AOTF (FBG-AOTF) which is also named as FBG based acousto-optic superlative modulator has been proposed by Liu *et. al* [17], the research in the FBG-AOTF has a great development [18]–[24]. Because the spectrum can be controlled by the acoustic wave (AW), the FBG-AOTF can be widely applied in add-drop multiplexer [25], fiber laser [26], and grating writing [27].

In this paper, we propose a novel FMF tunable mm-wave signal generation approach by employing a uniform fiber Bragg grating based acousto-optic tunable filter (UFBG-AOTF). It should be noted that only one dual-driving MZM (DD-MZM) is used in the proposed scheme. The filter is realized by launching an axially propagating AW into a UFBG. The center wavelength and the reflected power of this AOTF could be tuned by adjusting the frequency and the magnitude of the applied AW signals, respectively [17], [22]. In the experiment, two AOTFs with different reflective characteristics are made. After applying such homemade filters, the FMF of the mm-wave signals can be tuned from 2 to 4. In addition, with the AW frequency increasing, higher FMFs such as 6, 8 and 10 are obtained as shown in numerical simulations. Moreover, the 256 Mbit/s data can be successfully transmitted through a standard mode fiber (SMF) of 25km with a low power penalty.

2. Principles of the UFBG-AOTF

As shown in the Fig. 1, the UFBG-AOTF [18] is composed of a uniform fiber Bragg grating (UFBG), a silica horn and a shear-mode piezoelectric ceramic transducer (PZT). To enhance the effectiveness of the AW coupling into the UFBG, the UFBG cladding is etched by the hydrofluoric acid and the cladding diameter is decreased from 125 μm to 60 μm. The shear-mode PZT paralleled to the fiber driven by an electric signal creates a longitudinal vibration along the fiber axis causing compression and expansion on the UFBG periodically. The strain field of the longitudinal vibration could be written as

$$s(z) = s_0 \sin(k_a z), \quad k_a = 2\pi/\lambda_a \tag{1}$$

where k_a is the propagation constant of the AW, $\lambda_a = v_a/f_a$ is the acoustic wavelength, v_a is the acoustic phase velocity, f_a is the acoustic frequency, and s_0 is the amplitude of acoustically induced

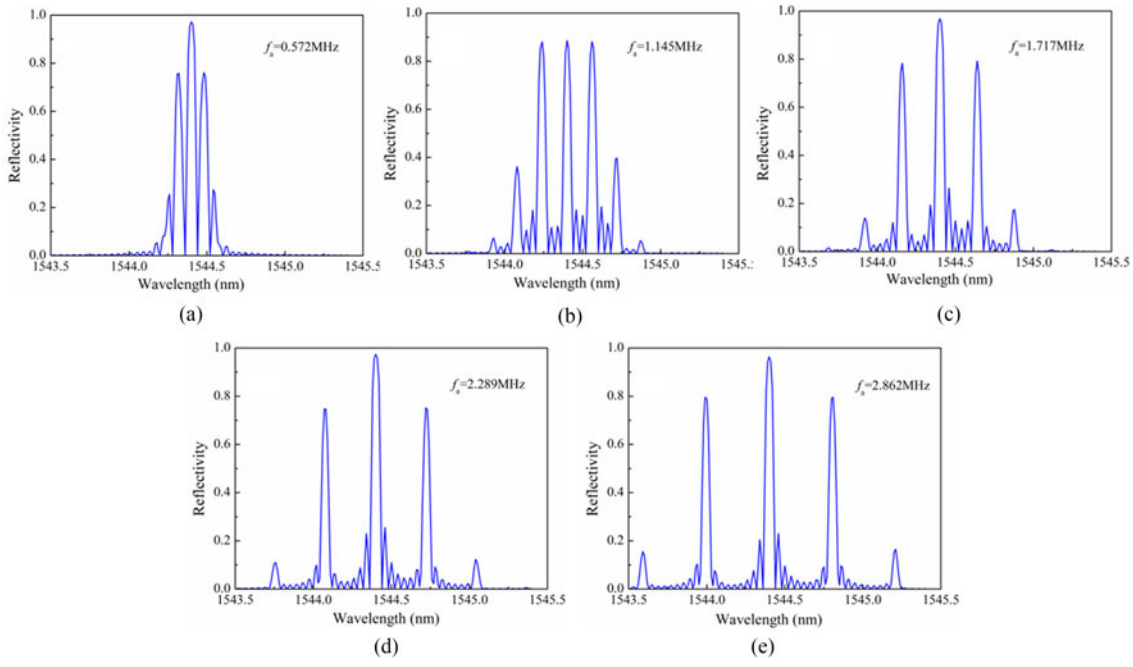

Fig. 2. Simulated FBG reflected spectra with AW of different frequency (f_a) applied. (a) 0.572 MHz, (b) 1.145 MHz, (c) 1.717 MHz, (d) 2.289 MHz, and (e) 2.862 MHz.

strain that determined by the diameter of the optical fiber and the strength of the AW. For the fiber with a cross-sectional area A, Young's modulus E and acoustic group velocity v_{ga}, carrying power P_a of the AW inside, the s_0 could be expressed as

$$s_0 = \sqrt{2P_a/(EAv_{ga})}. \tag{2}$$

After propagating over the grating, the AW is absorbed by the fiber coating layer and the fiber holders which are used for fixing the UFBG-AOTF. Due to the longitudinal vibration of the grating, the refractive index of the grating n is changed, which expressed as

$$n^2 = n_0^2 + 2\delta n \cos[kz + a\sin(k_a z)] = J_0(a)\cos(kz) + \sum_{i=1}^{\infty} J_i(a) \times \left[\cos(kz + ik_a z) + (-1)^i \cos(kz - ik_a z)\right] \tag{3}$$

where δn is the modulated depth of the grating refractive index, $\boldsymbol{k} = 2\pi/\Lambda$ is the grating vector, Λ is the period of the grating, $a = ks_0/k_a$ is the modulated depth of AW, and $J_i(.)$ is the Bessel function of the first kind of order i.

Simulations are carried out to investigate the reflective characteristic of the UFBG-AOTF. The parameters of the UFBG in the simulation are shown as follows: $\lambda = 1544.40$ nm, $n = 1.4628$, $\Lambda = 527.89$ nm, $L = 2.0$ cm, $\delta n = 0.8 * 10^{-4}$, in which L and λ are the length and the central wavelength of the grating, separately. Fig. 2 shows the simulated spectra of the FBGs, when the frequencies of applied AWs are 0.572 MHz, 1.145 MHz, 1.717 MHz, 2.289 MHz, and 2.862 MHz, separately. Simulation results indicate that compared with the unmodulated UFBG, which only has one primary reflected peak, more reflections appear in the spectra of the modulated ones. Note that, the location of the primary reflected peak is independent of AW. The secondary reflected peaks are symmetrically located around the primary one. Acoustic frequency can change the location of secondary reflected peaks, while the acoustically induced strain s_0 can change the energy distribution among the primary and secondary reflections.

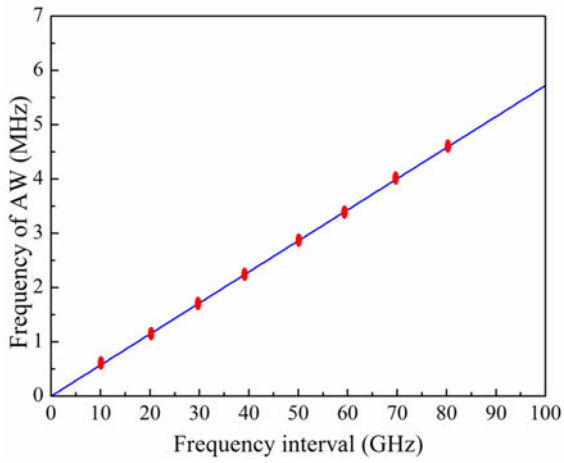

Fig. 3. Numerically calculated relationship between f_a and frequency interval.

The wavelength space between the primary and secondary reflected peaks is proportional to the frequency of AW. The proportional factor is 0.14 nm/MHz [21], [27]. This relation can be used to choose the AW frequency when the RF modulating signal in the RoF system is given. According to numerical calculation, when the secondary reflected peaks align to the target sidebands of the output signal from the modulator, the relationship between the frequency of applied AW and the frequency interval is depicted by Fig. 3. Here, the frequency interval refers to the frequency space between the optical carrier and sidebands. When the frequency intervals are 10 GHz, 20 GHz, 30 GHz, 40 GHz, and 50 GHz, separately, the corresponding frequencies of the AW are the ones listed in Fig. 2.

3. Mechanism of the Scheme

3.1 Operation Principle

The conceptual diagram of the proposed FMF tunable mm-wave signal generation method is shown in Fig. 4. A continuous lightwave is generated by a tunable laser (TL) and then injected into the DD-MZM. The multiplication of the RF signal and the baseband signal *S(t)* acts as the driving signal of the DD-MZM. The DD-MZM is biased at its quadrature bias point, and the phase difference between the two RF branches is π to realize optical double-sideband modulation. The output optical field E_{out} of the DD-MZM can be expressed as

$$\begin{aligned} E_{out}(t) &= E_{in}(t)\left\{\begin{array}{l} J_0(m)+2\sum_{n=1}^{\infty}(-1)^n J_{2n}(m)cos2n\Omega t \\ -2\sum_{n=0}^{\infty}(-1)^n J_{2n+1}(m)cos(2n+1)\Omega t \end{array}\right\} \\ &= S(t)\cdot E_0\exp(j\omega t)\left\{\begin{array}{c} J_0(m)-2J_1(m)cos\Omega t-2J_2(m)cos2\Omega t \\ +2J_3(m)cos3\Omega t+2J_4(m)cos4\Omega t \\ -2J_5(m)cos5\Omega t+..... \end{array}\right\} \end{aligned} \quad (4)$$

where E_0 and ω represent the amplitude and center angular frequency of the input optical signal, respectively. $m = \pi V_{RF}/V_\pi$ is defined as the modulation index of the MZM. Ω and V_{RF} denote the frequency and voltage magnitude of the RF modulation signal, respectively. V_π is the half-switch voltage of the MZM. $J_n(.)$ is the Bessel function of first kind of order n.

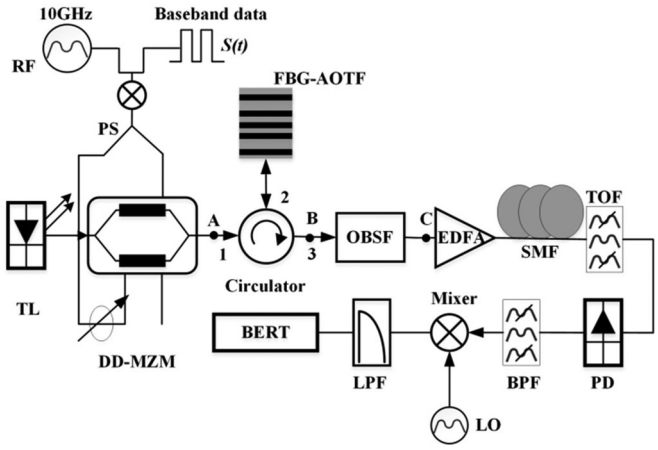

Fig. 4. Schematic diagram of the proposed FMF tunable mm-wave signal generation method. (TL: tunable laser, DD-MZM: Dual-driving Mach-Zehnder modulator; OBSF: optical bandstop filter; PD: photodetector, TOF: tunable optical filter, BPF: band pass filter, LPF: low pass filter, BERT: bit-error-rate tester.)

We can adjust m to make sure that the power of the required sidebands is large enough. Under the condition of appropriate m, the fifth-order sidebands still have considerable amplitude, and the harmonics higher than J_5 can be neglected without significant error. The optical field can be further written as

$$E_{out}(t) \approx S(t) \cdot E_0 \left\{ \begin{array}{l} J_0(m)exp(j\omega_0 t) - J_1(m)exp\,[j(\omega_0+\Omega)t] \\ -J_1(m)exp[-j(\omega_0-\Omega)t] - J_2(m)exp\,[j(\omega_0+2\Omega)t] \\ -J_2(m)exp\,[j(\omega_0-2\Omega)t] + J_3(m)exp\,[j(\omega_0+3\Omega)t] \\ +J_3(m)exp\,[j(\omega_0-3\Omega)t] + J_4(m)exp\,[j(\omega_0+4\Omega)t] \\ +J_4(m)exp\,[j(\omega_0-4\Omega)t] - J_5(m)exp\,[j(\omega_0+5\Omega)t] \\ -J_5(m)exp\,[j(\omega_0-5\Omega)t] \end{array} \right\}. \quad (5)$$

It can be seen from (5) that the output of the DD-MZM is composed of the optical carrier and symmetric sidebands of each-order. This output signal is injected into an optical circulator from port 1, and the UFBG-AOTF is connected with port 2. AW signals are applied on the PZT with certain frequency according to the relationship between the frequency of the AW and the RF signal shown by Fig. 3. Since the primary and two secondary reflected peaks appear in the spectrum of the FBG-AOTF, the optical carrier and two sidebands which are aligned with the primary and secondary reflected peaks can be output from port 3. An optical band-stop filter (OBSF) which is connected to port 3 is used to remove the optical carrier. The signal which is composed of two sidebands is then amplified by an erbium-doped fiber amplifier (EDFA) before it is transmitted over various lengths of SMFs. After the detection by a photodetector (PD), mm-wave with a FMF of $2n$ ($n = 1, 2, 3, 4, 5$) can be generated. We use an electrical LO and a mixer to down-convert the electrical mm-wave signal. And the bit-error-rate (BER) performance is evaluated by a BER tester.

3.2 Simulation Setup and Results

In order to verify our proposed scheme, a simulation system is built up based on the Optisystem 10.0 [28], [29] platform as shown in Fig. 4. The output of the tunable laser has a central wavelength of 1544.4 nm, which is identical with the central wavelength of the UFBG-AOTF. The DD-MZM is set at its quadrature bias point to realize optical double-sideband modulation with a modulation index of $m = \pi$. The frequency of the RF modulating signal and the baseband signal

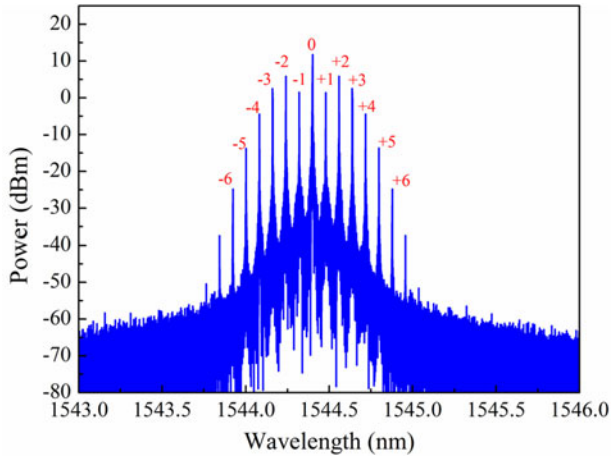

Fig. 5. Spectrum of the output optical frequency comb from the DD-MZM.

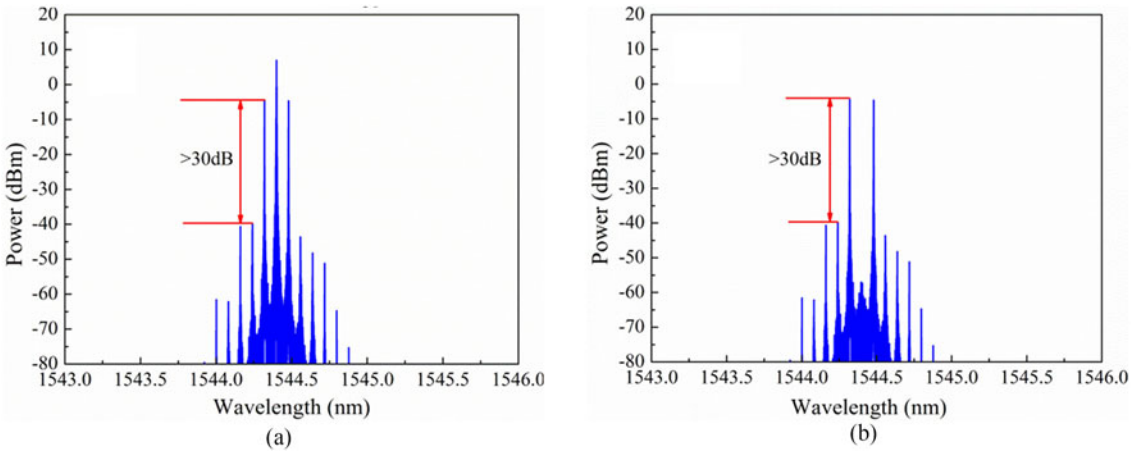

Fig. 6. Optical spectrum of the signal at: (a) point B and (b) point C.

are 10 GHz and 256 Mbit/s separately, and the output signal of the DD-MZM is shown by Fig. 5. It can be seen that the ±5th-order sidebands still have considerable amplitudes, just as expected. After transmission through the AOTF, whose reflection characteristic is depicted by Fig. 2(a), both optical carrier and the ±2nd sidebands are reflected. The spectrum of the output signal from port 3 (point B) of the circulator is shown by Fig. 6(a). It can be found that the extinction ratio is higher than 30 dB. An inverted Gaussian OBSF is connected behind the circulator to filter out the optical carrier of the signal at point B; thus, its central wavelength should be also set as 1544.40 nm. Under this situation, the output spectrum of the OBSF (point C) is shown in Fig. 6(b). Then, the signal was amplified in an EDFA with a gain of 3 dB. Finally, after the process of photo-detection, the mm-wave with a FMF of 2 is generated, shown by Fig. 7(a). By tuning the applied AW frequency from 0.572 MHz to 1.145 MHz, 1.717 MHz, 2.289 MHz, and 2.862 MHz separately, the mm-wave with FMFs of 4, 6, 8, and 10 are generated at the output of PD, as shown in Fig. 7(b)–(e).

The BER performance for the data of 256Mbit/s after transmission through SMFs of 0 km and 25 km are shown in Fig. 8, under the condition that the FMFs are 2 and 4, separately. It can be found that, after transmission over SMF of 25 km, the power penalty of the links are 2.80 dB and 2.64 dB separately because of dispersion in SMF.

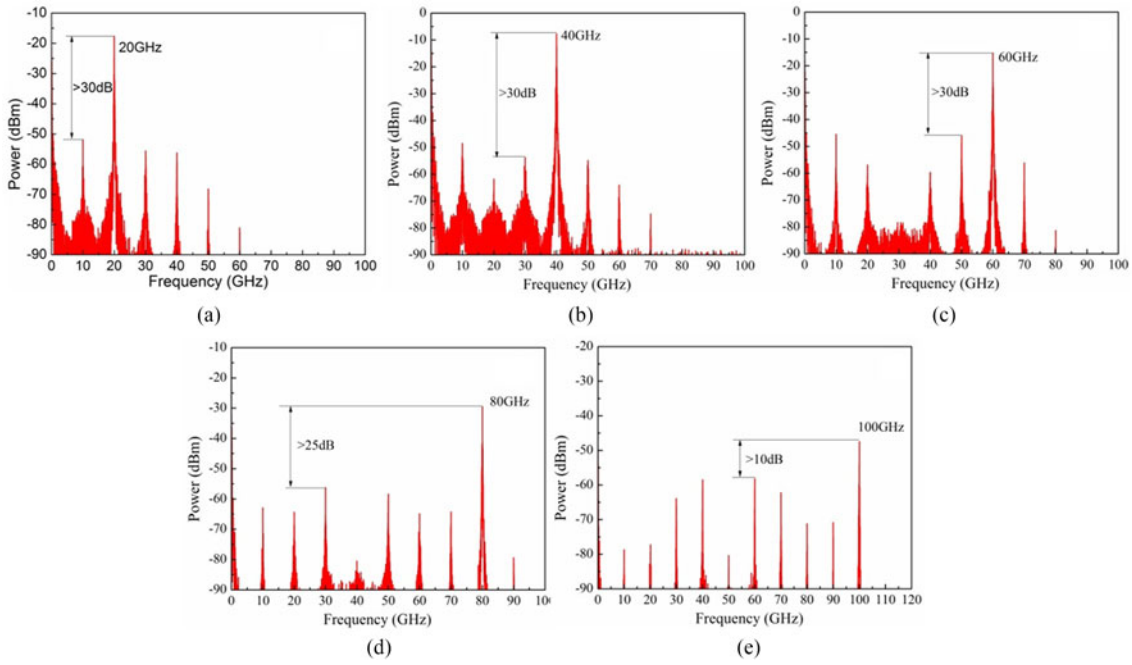

Fig. 7. Electrical spectra of the generated mm-wave signals with FMFs of (a) 2, (b) 4, (c) 6, (d) 8, and (e) 10.

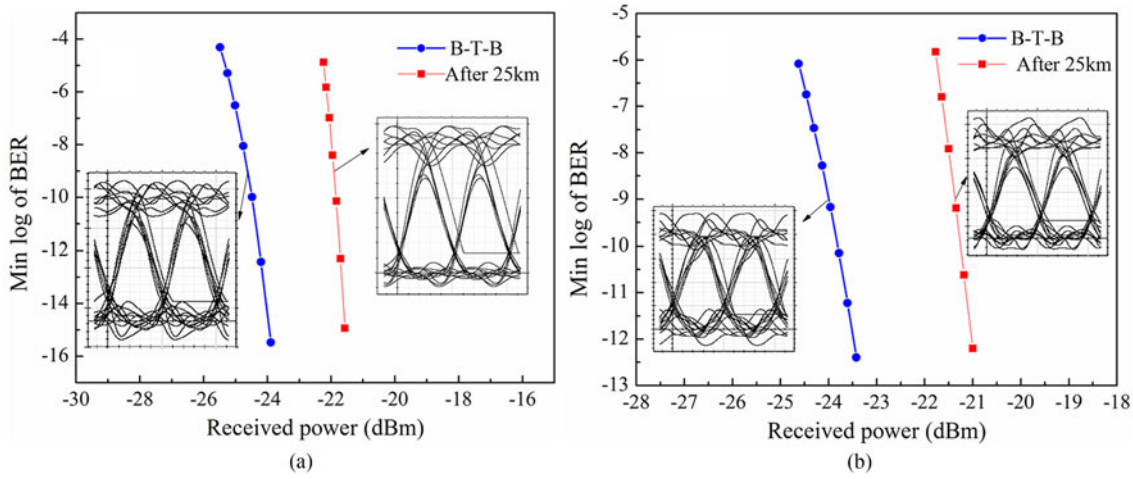

Fig. 8. BER curves and the eye diagrams of the signal at different transmission distances when the FMF is (a) 2 and (b) separatly.

3.3 mm-Wave Generation by Employing Home-Made FBG-AOTFs

Experiments are also implemented to study the performance of the UFBG-AOTF. The experimental setup is the same as Fig. 1. The UFBG has a reflectivity of 97% and the center wavelength is 1544.40 nm. The longitudinal AW is amplified by a conic silica horn attached on the top surface of the shear-mode PZT plate, and the tip of silica horn is glued to a point of single-mode fiber (SMF) located about 2 cm away from UFBG. The reflection spectra of UFBG are measured by a broadband ASE light source and an ANDO AQ6317C optical spectrum analyzer (OSA) with a resolution of 0.01 nm.

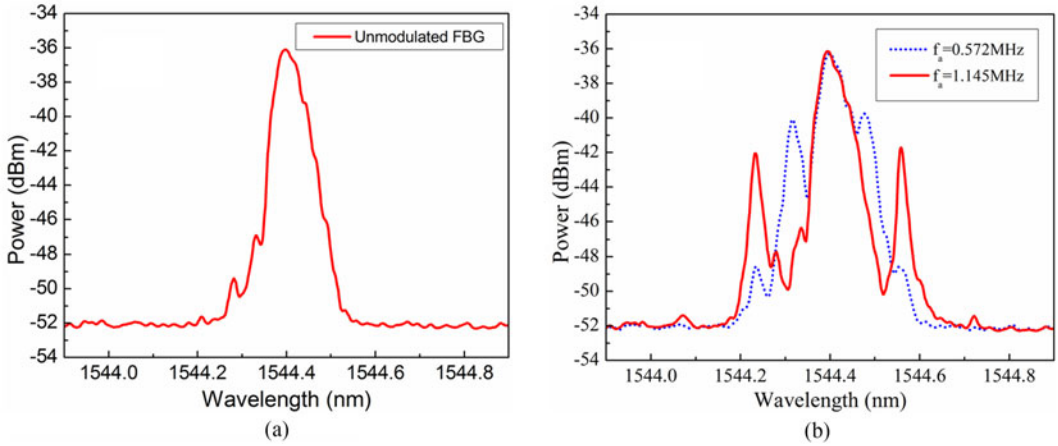

Fig. 9. Experimentally measured reflection spectrum of (a) the uniform FBG before modulated by AW. (b) FBGs driven by AWs of 0.572 MHz and 1.145 MHz separately.

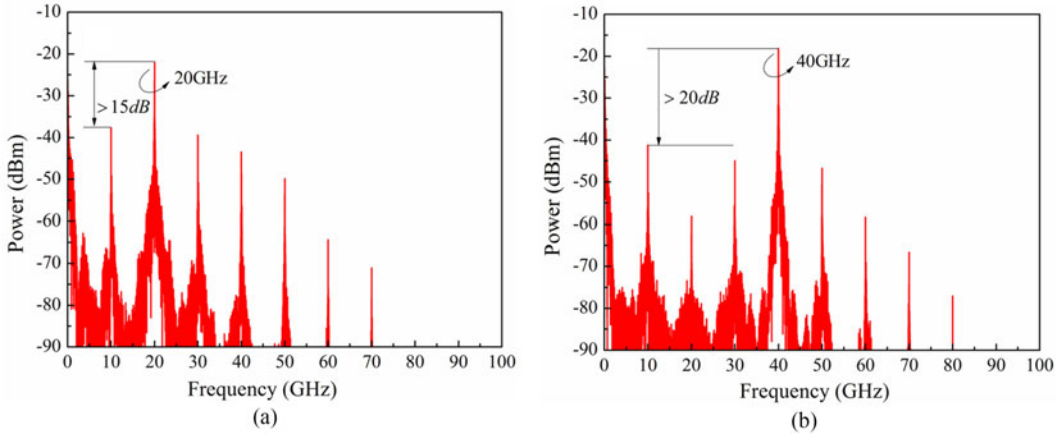

Fig. 10. Electrical spectra of the generated mm-wave signals with FMFs of 2 and 4 by employing the homemade UFBG-AOTFs.

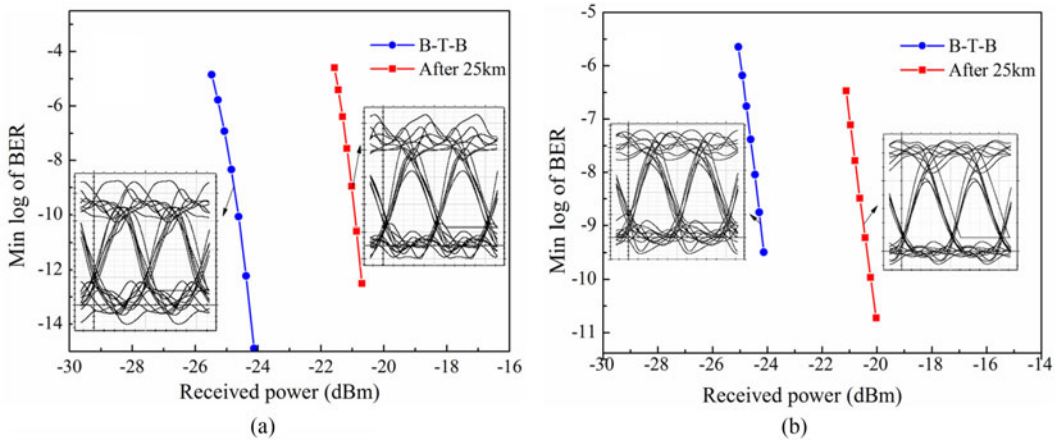

Fig. 11. BER curves and the eye diagrams of the signal at different transmission distances when the FMF is (a) 2 and (b) 4 separately by employing the homemade UFBG-AOTFs.

It is obviously shown in the Fig. 9(a) that there exists only one reflection peak in the measured reflective spectrum of the UFBG before it is modulated by the AW. Then, when AWs at two different frequencies (0.572 MHz and 1.145 MHz) are applied, the spectra of the AOTFs are shown in Fig. 9(b). As mentioned before, the wavelength space between the primary and secondary reflection peak is proportional to the AW frequency. In our practical work, the proportional factor is calculated as 0.142 nm/MHz, which is quite in close agreement with the theoretical value 0.14 nm/MHz.

By applying the two homemade FBG-AOTFs in the whole system built by the Optisystem, the electrical spectra of the generated mm-waves with FMFs of 2 and 4 are shown in Fig. 10. Although the obtained electrical sideband suppression ratio by the homemade FBG-AOTFs are lower than that in Fig. 7, the values ($>$15 dB) are already enough for need of the basic communication.

Under this condition, the BER performance for the signal data after transmission through SMFs of 0 km and 25 km are also evaluated, which is shown by Fig. 11. The corresponding power penalties are 3.77 dB and 3.72 dB separately.

4. Conclusions

A millimeter-wave signal generation with tunable frequency multiplication factor employing UFBG-AOTF has been proposed and demonstrated. By applying two homemade UFBG-AOTFs into the system built by the Optisystem, the mm-wave with FMF of 2 and 4 can be achieved. We also verify the realization of FMF $=$ 6, 8, 10 by simulation. Since the scheme realizes the tunability of FMFs by choosing the appropriate AW frequency applied on the PZT, it reduces the frequency requirement of the modulator and the oscillator greatly. This method provides a simple, convenient, and low-cost way to generate mm-wave with different FMFs. In addition, higher FMF can be achieved by increasing the modulation index of the DD-MZM.

References

[1] L. Zhang *et al.*, "OFDM modulated WDM-ROF system based on PCF-supercontinuum," *Opt. Exp.*, vol. 18, pp. 15003–15008, 2010.

[2] Z. Jia, J. Yu, G. Ellinas, and G. K. Chang, "Key enabling technologies for optical-wireless networks: Optical millimeter-wave generation, wavelength reuse, and architecture," *J. Lightw. Technol.*, vol. 25, no. 11, pp. 3452–3471, Nov. 2007.

[3] K. Xu *et al.*, "Microwave photonics: Radio-over-fiber links, systems, and applications [Invited]," *Photon. Res.*, vol. 2, pp. B54–B63, 2014.

[4] M. Sauer, A. Kobyakov, and J. George, "Radio over fiber for picocellular network architectures," *J. Lightw. Technol.*, vol. 25, no. 11, pp. 3301–3320, Nov. 2007.

[5] D. Wake, A. Nkansah, and N. J. Gomes, "Radio over fiber link design for next generation wireless systems," *J. Lightw. Technol.*, vol. 28, no. 16, pp. 2456–2464, Aug. 2010.

[6] I. Aldaya, G. Campuzano, and G. Castañón, "Simultaneous generation of wavelength division multiplexing PON and RoF signals using a hybrid mode-locked laser," *Opt. Fiber Technol.*, vol. 23, pp. 53–60, 2015.

[7] J. Yao, "Microwave photonics," *J. Lightw. Technol.*, vol. 27, no. 3, pp. 314–335, Feb. 2009.

[8] Q. Guohua, Y. Jianping, J. Seregelyi, S. Paquet, and C. Belisle, "Generation and distribution of a wide-band continuously tunable millimeter-wave signal with an optical external modulation technique," *IEEE Trans. Microw. Theory Techn.*, vol. 53, no. 10, pp. 3090–3097, Oct. 2005.

[9] Y. Jianjun *et al.*, "Optical millimeter-wave generation or up-conversion using external modulators," *IEEE Photon. Technol. Lett.*, vol. 18, no. 1, pp. 265–267, Jan. 2006.

[10] J. Lu, Z. Dong, L. Chen, J. Yu, and S. Wen, "High-repetitive frequency millimeter-wave signal generation using multi-cascaded external modulators based on carrier suppression technique," *Opt. Commun.*, vol. 281, pp. 4889–4892, 2008.

[11] C.-T. Lin *et al.*, "Generation of carrier suppressed optical mm-wave signals using frequency quadrupling and no optical filtering," in *Proc. Optical Fiber Commun. Conf./Nat. Fiber Opt. Eng. Conf.*, San Diego, CA, USA, 2008, Paper JThA73.

[12] J. Ma *et al.*, "Optical millimeter wave generated by octupling the frequency of the local oscillator," *J. Opt. Netw.*, vol. 7, pp. 837–845, 2008.

[13] C.-T. Lin *et al.*, "A continuously tunable and filterless optical millimeter-wave generation via frequency octupling," *Opt. Exp.*, vol. 17, pp. 19749–19756, 2009.

[14] Y. Chen, A. Wen, J. Guo, L. Shang, and Y. Wang, "A novel optical mm-wave generation scheme based on three parallel Mach–Zehnder modulators," *Opt. Commun.*, vol. 284, pp. 1159–1169, 2011.

[15] X. Yin, A. Wen, Y. Chen, and T. Wang, "Studies in an optical millimeter-wave generation scheme via two parallel dual-parallel Mach–Zehnder modulators," *J. Modern Opt.*, vol. 58, pp. 665–673, 2011.

[16] W. Zhang *et al.*, "Tunable broadband light coupler based on two parallel all-fiber acousto-optic tunable filters," *Opt. Exp.*, vol. 21, pp. 16621–16628, 2013.

[17] W. F. Liu, P. S. J. Russell, and L. Dong, "Acousto-optic superlattice modulator using a fiber Bragg grating," *Opt. Lett.*, vol. 22, pp. 1515–1517, 1997.
[18] C. Liu *et al.*, "Characteristics of the fiber Bragg grating based all-fiber acousto-optic modulator," *Acta Physica Sinica*, vol. 62, 2013, Art. no. 034208.
[19] C. A. F. Marques *et al.*, "Acousto-optic effect in microstructured polymer fiber Bragg gratings: Simulation and experimental overview," *J. Lightw. Technol.*, vol. 31, no. 10, pp. 1551–1558, May 2013.
[20] R. E. Silva, M. A. R. Franco, P. T. Neves, H. Bartelt, and A. A. P. Pohl, "Detailed analysis of the longitudinal acousto-optical resonances in a fiber Bragg modulator," *Opt. Exp.*, vol. 21, pp. 6997–7007, 2013.
[21] R. A. Oliveira, P. T. Neves Jr, J. T. Pereira, and A. A. P. Pohl, "Numerical approach for designing a Bragg grating acousto-optic modulator using the finite element and the transfer matrix methods," *Opt. Commun.*, vol. 281, pp. 4899–4905, 2008.
[22] Z. Li, L. Pei, C. Liu, T. Ning, and S. Yu, "Research on FBG-based longitudinal-acousto-optic modulator with Fourier mode coupling method," *Appl. Opt.*, vol. 51, pp. 7314–7318, 2012.
[23] D. I. Yeom, H. S. Park, and B. Y. Kim, "Tunable narrow-bandwidth optical filter based on acoustically modulated fiber Bragg grating," *IEEE Photon. Technol. Lett.*, vol. 16, no. 5, pp. 1313–1315, May 2004.
[24] L.-Y. Wu *et al.*, "Spectral analysis of the UFBG-based acousto-optical modulator in V-I transmission matrix formalism," *Chin. Phys. B*, vol. 23, 2014, Art. no. 110702.
[25] A. Diez, M. Delgado-Pinar, J. Mora, J. Cruz, and M. Andrés, "Dynamic fiber-optic add-drop multiplexer using Bragg gratings and acousto-optic-induced coupling," *IEEE Photon. Technol. Lett.*, vol. 15, no. 1, pp. 84–86, Jan. 2003.
[26] M. Delgado-Pinar, D. Zalvidea, A. Diez, P. Perez-Millan, and M. Andres, "Q-switching of an all-fiber laser by acousto-optic modulation of a fiber Bragg grating," *Opt. Exp.*, vol. 14, pp. 1106–1112, 2006.
[27] R. A. Oliveira *et al.*, "Complex Bragg grating writing using direct modulation of the optical fiber with flexural waves," *Appl. Phys. Lett.*, vol. 99, 2011, Art. no. 161111.
[28] J. Li *et al.*, "Quasi-optical single-sideband modulation with continuous carrier-to-sideband ratio tunability," *Chin. Opt. Lett.*, vol. 13, 2015, Art. no. 080606.
[29] A. O. Aldhaibani *et al.*, "2.5 Gb/s hybrid WDM/TDM PON using radio over fiber technique," *Optik–Int. J. Light Elect. Opt.*, vol. 124, pp. 3678–3681, 2013.